Microchemical Journal 218 (2025) 115322

Contents lists available at ScienceDirect

Microchemical Journal

journal homepage: www.elsevier.com/locate/microc

NH2-MIL-101(Cr)/SBA15 nanocomposite as sorbent in syringe-filter-SPE for determination of pesticides in environmental water

Soleyman Moinfar [a,b,*], Ali Khodayari [c], Aveen Mustafa Mohammed [d], Eslam Pourbasheer [c], Ali Aghaei [e]

[a] Chemical Analysis Research Center, Scientific Research Center, University of Zakho, Zakho, Iraq
[b] Department of Basic Sciences, College of Pharmacy, Nawroz University, Duhok, Iraq
[c] Department of Chemistry, Faculty of Science, University of Mohaghegh Ardabili, 56199-11367 Ardabil, Iran
[d] Department of Chemistry, College of Science, University of Duhok, Duhok 42001, Iraq
[e] Konax BV, Izegem, Belgium

ARTICLE INFO

Keywords:
Syringe-filter solid-phase extraction
Environmental water
Pesticides
NH_2-MIL-101(Cr)/SBA nanocomposite
HPLC-PDA

ABSTRACT

Determination of low-concentration pesticides in real samples requires a simple, rapid, low-solvent-consumption, and high-efficiency extraction method before introduction into the chromatography system. In the present research, the objectives mentioned were achieved by using the developed NH2-MIL-101(Cr)/SBA-15 nanocomposite with high extraction efficiency as a sorbent in the syringe filter–solid-phase extraction (SPE) approach, which is easy to use and has low solvent consumption. In this study, for the first time, the metal–organic framework NH2-MIL-101(Cr) was combined with Santa Barbara Amorphous-15 (SBA-15) and was used as sorbent in syringe filter-SPE for extracting some pesticides from environmental water samples. To verify the successful formation of the nanocomposite, several characterization techniques including SEM, FTIR, XRD, TGA, and BET were employed. Furthermore, the variables affecting the extraction efficiency of NH2-MIL-101(Cr)/SBA-syringe - filter-SPE-HPLC, such as the sample volume, pH, volume of eluting solvent, and type of eluting solvent were optimized by utilizing a response surface methodology (RSM) based on central composite design (CCD). The results demonstrated that the NH_2-MIL-101(Cr)/SBA-15 composite exhibited superior adsorption performance and lower detection limits for the target pesticides compared to the unmodified NH_2-MIL-101(Cr). The method achieved detection limits ranging from 0.07 to 0.6 μg/L, with a linear response range of 0.25 to 800.0 μg/L. It also showed strong repeatability, with relative standard deviation (RSD) values between 2.8 % and 5.0 %, and excellent recovery rates of 90 % to 105 % at spiked concentrations from 2.0 to 40.0 μg/L.

1. Introduction

Insecticides are highly essential pesticides that are commonly used to protect crops, forests, and agricultural products from insects [1,2]. Neonicotinoids (NEOs) are a class of synthetic insecticides used to control pests in agriculture, horticulture, and residential settings due to their effectiveness against a wide range of insects.

According to a 2020 report, NEOs were the leading products in the global insecticide market [3]. As a result, neonicotinoids have gained significant popularity and now account for nearly one-third of the global insecticide market [4]. The widespread use of pesticides has posed serious risks to human health and the environment; some researches have shown that NEOs can induce embryotoxicity, breast cancer, congenital heart defects and autism spectrum disorders [3,5]. Several studies have shown that bees, birds, and butterflies neonicotinoid may be exposed to residual insecticides, which affect their behavior, nutrient metabolism, and immune system and can significantly reduce the their populations [4,6,7]. Carbendazim ($C_9H_9N_3O_2$; CBZ) is a benzimidazole fungicide known for its cost-effectiveness and widespread use in controlling various diseases in fruit and vegetable crops during both the pre-harvest and post-harvest stages [8]. Nevertheless, CBZ has a half-life of over 25 months under anaerobic conditions, highlighting its significant persistence as a contaminant in the environment. This underscores the need for developing sensitive and selective methods for detecting CBZ to protect the environment and safeguard human health [9].

A major concern with pesticide use is their contamination of water

* Corresponding author at: Chemical anlysis research center, Scientific research center, University of Zakho, Zakho, Iraq.
E-mail address: soleiman_moinfar@yahoo.com (S. Moinfar).

https://doi.org/10.1016/j.microc.2025.115322
Received 20 July 2025; Received in revised form 11 September 2025; Accepted 12 September 2025
Available online 13 September 2025

sources, including both surface and groundwater, which adversely affects water quality and poses risks to human health. Pesticide-induced water pollution results from agricultural activities, urban usage, and pesticide manufacturing facilities [10]. To ensure human health safety, it is necessary to regulate the water quality before consumption. Consequently, the European Union has set maximum allowable concentrations for pesticides and their degradation products at 0.1 and 0.5 μg/L in surface and groundwater, respectively [11,12]. Due to the extremely low maximum residue limit (MRL) values of pesticides in environmental samples, and the potential for complex matrix interference, extraction and preconcentration of the analytes are crucial before analysis. Accurate and sensitive detection of target analytes requires a sample preparation procedure with high preconcentration efficiency [13–15].

Various preconcentration methods have been employed to increase the concentration of pesticides before analysis, including solid-phase extraction (SPE) [7], heat-induced homogeneous liquid-liquid microextraction [16], solid-phase microextraction (SPME) [5], and QuEChERS (quick, easy, inexpensive, effective, rugged, and safe) [17], magnetic solid phase extraction (MSPE) [8], and dispersed liquid-liquid microextraction (DLLME) [9]. The methods mentioned above, such as DLLME with high enrichment factor and high speed, QuEChERS with high extraction efficiency for food samples, SPME solventless consumption and low detection limit, and SPE and MSPE with low solvent consumption and high extraction efficiency, have been used many times for the extraction and preconcentration of various analytes. However, majority of these techniques methods, despite their numerous benefits, are hindered by limitations like inadequate adsorbents stability, elevated backpressure, slow diffusion and mass transfer rates, the need for substantial amounts of desorbing solvent, and in some cases, small sample volumes [18]. Traditional solid-phase extraction (SPE) remains a widely adopted technique for sample pretreatment, but it, while simple, suffers from several limitations that hinder its overall efficiency and broader application. These include lengthy processing times, column clogging and back pressure, complex cartridge preparation, and the need for large volumes of solvent to elute analytes [19].

To overcome these challenges, our group developed the syringe filter-SPE over the past two years. This approach significantly improves upon traditional SPE by offering advantages such as rapid and straightforward MOF-sorbent integration into syringe filter, shorter extraction times, higher efficiency, reduced solvent usage, minimal sorbent requirement, and the elimination of back pressure during sample flow [20,21]. Given the critical role of sorbents in enhancing the extraction of target compounds, there has been growing interest in developing novel, high-performance adsorbents for sample preparation [22], and in this work, we attempted to enhance the extraction efficiency by synthesis of a novel MOF-composite. One promising class of materials is metal-organic frameworks (MOFs)—hybrid structures made of metal ions or clusters linked by organic ligands, forming a highly porous three-dimensional network. MOFs are widely used in analytical applications due to their large surface area, tunable pore sizes, thermal stability, and chemical adaptability [19,20]. Notably, MOFs have shown excellent potential for pesticide residue extraction, outperforming many conventional sorbents. Their effectiveness is largely due to strong host–guest interactions that facilitate the retention of analytes, thereby enabling high sample loading capacities even in complex matrices [19].

Previous work by our team demonstrated the use of a GNP/MIL-101 (Cr) composite in the same SPE format for extracting organophosphate pesticides [20]. Additionally, the effectiveness of various MOFs—including AlFu, IRMOF-3, NH_2-MIL-101(Al), NH_2-MIL-101(Cr), and MIL-53(Al) was previously evaluated for the extraction of antibiotics using the syringe filter-SPE approach. Although syringe filter-SPE offers several benefits, including low adsorbent and solvent consumption, rapid adsorption and desorption steps, and the quick, cost-effective preparation of filters containing the adsorbent, making it a practical and efficient alternative to traditional SPE methods. However, the extraction efficiency and performance of the method depend on the sorbent properties. Therefore, to further enhance the extraction performance, new NH_2-MIL-101(Cr)-based composites were synthesized and employed as adsorbents in a syringe filter-SPE for the extraction and preconcentration of pesticides from water samples. NH_2-MIL-101(Cr) was selected for this study due to its high adsorption capacity and its ability to allow smooth passage of aqueous samples without generating backpressure. For the first time, a novel composite incorporating Santa Barbara Amorphous-15 (SBA-15)—designated as NH_2-MIL-101(Cr)-SBA-15—was developed. SBA-15 was chosen due to its high surface area, excellent water stability, and strong affinity for organic compounds, making it an ideal additive for improving both adsorption capacity and extraction efficiency. The new NH_2-MIL-101(Cr)-SBA-15 composite was successfully synthesized and applied for the preconcentration of imidacloprid, carbendazim, acetamiprid and thiacloprid from contaminated water samples, followed by HPLC analysis. To determine the optimal conditions for pesticide adsorption, Response Surface Methodology (RSM) was used to systematically evaluate and optimize the key influencing variables.

2. Experimental

2.1. Chemicals and reagents

Kindly see the supplemental information (ESI) for specific information regarding the Chemicals and Reagents.

2.2. Apparatus

High-performance liquid chromatography (HPLC) was used to analyze the extracted pesticides, employing a Thermo Scientific C18 column (150 mm × 4.6 mm, 5 μm) maintained at 35 °C, and equipped with a photodiode array detector (Flexar, Perkin Elmer, USA). Separation was achieved using a gradient elution with HPLC-grade water (A) and acetonitrile (B) as the mobile phase components. The optimized conditions were as follows: Initial conditions: 21 % B; 0–1.0 min, 27 % B; 1.0–4.5 min, 38 % B; 4.5–9.5 min, 22 % B; 9.5–16 min; followed by 1.0 min of equilibration to return to the initial conditions. The mobile phase flow rate was maintained at 1.0 mL/min. A total of 20.0 μL of the sample was injected. UV detection was performed at 244 nm for imidacloprid and carbendazim, and at 280 nm for acetamiprid and thiacloprid.

Kindly see the supplemental information (ESI) for specific information regarding the other Apparatus.

2.3. Synthesis

2.3.1. Synthesis of the NH_2-MIL-101(Cr)/GO

To synthesize the NH_2-MIL-101(Cr)/GO nanocomposite, a modified procedure based on the NH_2-MIL-101(Cr) synthesis (Kindly see the supplemental information (ESI) for specific information regarding the synthesis of the NH2-MIL-101(Cr)) was followed. Initially, 0.15 g of graphene oxide (GO) (United Nanotech Innovation Company, India) was dispersed in 20 mL of deionized water and subjected to ultrasonic treatment for one hour to promote partial exfoliation of the GO sheets. This dispersion was then poured into a Teflon-lined autoclave, where 5 mmol of 2-aminoterephthalic acid (ABDC) and 5 mmol of chromium nitrate nonahydrate [$Cr(NO_3)_3{\cdot}9H_2O$] were added.

To initiate the reaction, 20 mL of 0.7 M sodium hydroxide solution was gradually introduced while stirring the mixture at 500 rpm for 1 h, ensuring thorough mixing and dispersion of all components. The autoclave was sealed and heated to 150 °C for 12 h to facilitate crystallization, followed by natural cooling to room temperature. The resulting solid was collected by centrifugation at 6000 rpm for 5 min, and the product was then thoroughly washed multiple times with deionized water, followed by DMF and methanol rinses to eliminate any unreacted or loosely bound organic substances. The final material was dried at

100 °C for 24 h in an oven, yielding the desired NH_2-MIL-101(Cr)/GO composite.

2.3.2. Synthesis of the NH_2-MIL-101(Cr)/SBA-15

The same procedure described in Section 2.5.4 was utilized to synthesize the NH2-MIL-101(Cr)/SBA Nano composite, with 0.15 g of SBA-15 (Kindly see the supplemental information (ESI) for specific information regarding the synthesis of the SBA-15) replacing the GO.

2.4. Preparation of syringe filter

Seven mg of each adsorbent (GO, SBA, NH_2-MIL-101(Cr), NH_2-MIL-101(Cr)/GO and NH2-MIL-101(Cr)/SBA) were individually dispersed in 2 mL of ultrapure water using an ultrasonic bath for 20 s. The resulting suspensions were then passed through Teflon syringe filters (0.45 μm pore size) using 2 mL syringes, allowing for uniform distribution of the MOF adsorbents and composites across the filter surface. To remove any potential contaminants, each filter was preconditioned by sequentially passing 4 mL of ultrapure water followed by 2 mL of acetonitrile. These prepared filters were subsequently employed for the extraction of target analytes from water samples.

2.5. Sample preparation

River water was collected from the Khabir River (Zakho) and well water was collected from Zakho city. Then real samples were centrifuged for ten minutes (5000 rpm) in order to remove any sediments and suspended particles. Initially, the pH of water samples were adjusted to 7.2 using 0.1 M HCl or 0.1 M NaOH solutions. Then, 35.0 mL of each sample was passed through a syringe filter packed with the NH2-MIL-101(Cr)/SBA as sorbent at a flow rate of 4 mL/min. Following sample loading, the syringe filter was rinsed with 1 mL of ultrapure water. The pesticides retained on the sorbent (NH2-MIL-101(Cr)/SBA) were subsequently eluted using 0.22 mL of an elution solvent mixture (80 % methanol and 20 % acetonitrile) applied via a 1-mL medical syringe at a flow rate of 1.5 mL/min. Finally, 20.0 μL of the eluate was injected for HPLC analysis.

2.6. Influencing factors and responses

Key variables influencing the efficiency of the syringe filter–SPE procedure were identified based on an extensive review of relevant literature [1–3]. Based on this, three continuous variables—sample solution volume, desorption solvent volume, and pH—along with one categorical variable—type of desorption solvent—were selected for further optimization.

To explore the effects of these parameters and their interactions, experiments were systematically planned using Design-Expert version 13.0. A Central Composite Design (CCD) approach was employed to optimize the selected factors and maximize extraction performance. For response evaluation, the combined peak areas of the four target compounds, as measured by HPLC, were used as the experimental response variable.

3. Results and discussion

3.1. Characterization

3.1.1. Evaluation and interpretation of FT-IR spectra

Fig. S1 presents the FT-IR spectra of Cr-MOF/GO, Cr-MOF/SBA-15, pristine Cr-MOF, and GO. In the spectrum of Cr-MOF, characteristic absorption bands appear at 3459 cm^{-1} and 3372 cm^{-1}, corresponding to the N—H stretching vibrations of the amine group attached to the aromatic ring [23]. Peaks at 1576 cm^{-1} and 1116 cm^{-1} are attributed to C═C and C—H stretching within the benzene rings [24,25]. Additionally, O–C–O asymmetric stretching is observed at 1432 cm^{-1} and 1392 cm^{-1}, while the bands at 1260 cm^{-1} and 768 cm^{-1} are related to C—N stretching and vibrations of di-substituted aromatic rings, respectively. The band near 598 cm^{-1} indicates Cr—O symmetric stretching, confirming the presence of metal–ligand coordination [26].

The absence of strong signals between 1680 and 1720 cm^{-1} suggests that the carboxyl (-COOH) groups in 2-aminoterephthalic acid are effectively coordinated with chromium ions, integrating into the MOF framework. For Cr-MOF/SBA-15, the appearance of an additional band at 1090 cm^{-1} corresponds to the Si–O–Si stretching vibration, characteristic of the silica structure [27].

In the GO spectrum, weak absorption bands at 1728 cm^{-1}, 1634 cm^{-1}, and 3435 cm^{-1} are attributed to C═O stretching, C═C vibrations within the carbon framework, and –OH stretching from surface-adsorbed water, respectively [28]. The FT-IR profile of Cr-MOF/GO confirms successful nanocomposite formation, showing all the distinctive peaks of Cr-MOF with overlapping features from GO, indicating effective integration of the two components.

3.1.2. Brunauer–Emmett–teller (BET) analysis

The surface area, pore size distribution, porosity type, and total pore volume of the synthesized MOF and its nanocomposites were characterized by nitrogen adsorption–desorption isotherm measurements at 77 K. Before analysis, all samples were subjected to vacuum heating at temperatures exceeding 200 °C for 6 h to eliminate any residual molecules trapped inside the pores. The nitrogen adsorption–desorption isotherms obtained (shown in Fig. S2) reveal that each sample exhibits a type I isotherm, indicative of microporous materials [29].

Of particular interest, the isotherms for Cr-MOF show two distinct secondary adsorption steps around relative pressures (P/P_o) of 0.1 and 0.2, which are possibly related to micropore window effects. The BET method was applied to quantify the specific surface areas and pore features, with detailed results presented in Table S1. The calculated average pore diameters confirm that both Cr-MOF and its nanocomposites have predominantly mesoporous structures [27].

It was observed that the Cr-MOF/GO and Cr-MOF/SBA composites exhibit reduced surface areas and total pore volumes compared to the original Cr-MOF. This decrease is likely due to the deposition of GO and SBA nanostructures on and within the Cr-MOF framework, partially blocking or filling some pores [25,30]. Despite this reduction, these composites maintain sufficiently high surface areas, making them promising candidates for the adsorption of organic contaminants.

3.1.3. XRD analysis

Fig. S3 shows the XRD spectra for Cr-MOF, GO, SBA, and their nanocomposites across the 2θ range of 5° to 50°. The Cr-MOF sample displays characteristic diffraction peaks at 9.04°, 16.7°, 24.9°, and 42.31°, matching well with previously published data [29,31]. In the Cr-MOF/SBA composite, besides the original Cr-MOF reflections, a distinct peak appears at 24.5°, which corresponds to the (002) plane of SBA [27]. Meanwhile, the Cr-MOF/GO nanocomposite exhibits an additional peak at 10.3°, associated with the (001) plane of graphene oxide [32]. The lack of any other unexpected peaks in the patterns confirms that both composites, Cr-MOF/SBA and Cr-MOF/GO, are free from significant crystalline contaminants.

3.1.4. TGA analysis

The thermal stability of the synthesized Cr-MOF, Cr-MOF/GO, and Cr-MOF/SBA Nano composites was investigated using TGA, with the resulting thermograms shown in Fig. S4. For Cr-MOF, the thermograms reveal an initial mass loss of 5.5 % between 30 and 175 °C, which is attributed to the loss of free guest water. A subsequent mass loss of 15.2 % occurs between 175 and 285 °C due to the loss of —OH groups and coordinated water molecules [33]. The most significant mass loss (about 51 %) occurs between 285 and 420 °C, which might be due to the thermal decomposition of 2-aminoterephthalates. At 700 °C, the residual mass is 28.3 % of the original weight, corresponding to chromium

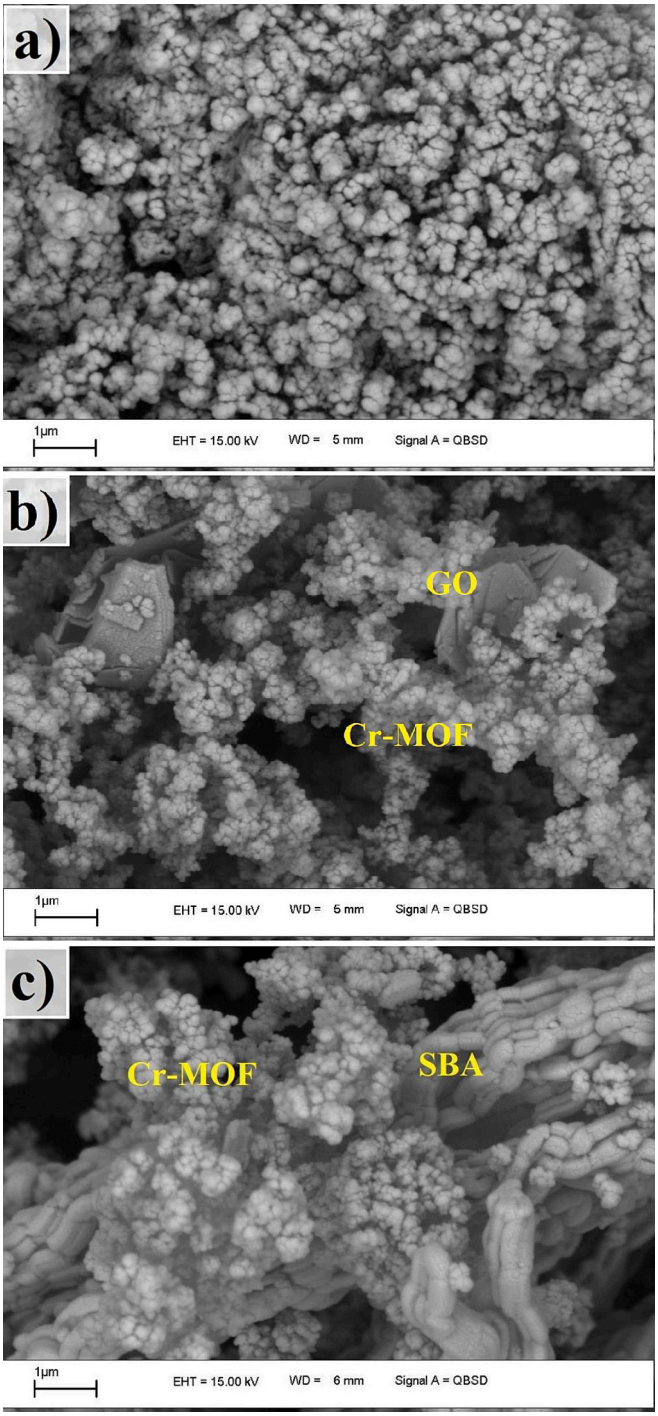

Fig. 1. SEM images of a) Cr-MOF, b) Cr-MOF/GO and c) Cr-MOF/SBA.

oxide. The TGA curve of Cr-MOF/GO nanocomposite shows an additional thermal event [34]. In this cae, a 10.4 % weight loss is observed between 420 and 700 °C, which is likely due to the gradual thermal degradation of GO in the nanocomposite. The thermogram of the Cr-MOF/SBA nanocomposite is similar to that of Cr-MOF, but with a higher residual mass of 38.1 % at 700 °C. This increased residual mass (9.8 % more than Cr-MOF) is attributed to the presence of stable SBA nanostructures within the Cr-MOF/SBA mixture. Overall, the TGA measurements indicate that the synthesized Cr-MOF and the produced nanocomposites are thermally stable up to temperatures of 280 °C.

3.1.5. SEM investigation

SEM was used to examine the morphology of the synthesized Cr-MOF and nanocomposites. Fig. 1a shows the SEM image of Cr-MOF, revealing quasi-spherical particles with diameters of approximately 30–80 nm, which aggregate into clusters with diameters ranging from 100 to 400 nm. Fig. 1b shows the SEM image of Cr-MOF/GO nanocomposite, where several GO sheets are distributed among the Cr-MOF crystals, indicating the presence of GO layers within the composite.

In Fig. 1c, the SEM image of the Cr-MOF/SBA nanocomposite shows Cr-MOF particles alongside SBA particles, which appear as intertwined filamentous tubes. The MOF particles are observed on the surface of these SBA structures.

3.2. Optimization by central composite design

A central composite design was employed for three numerical factors and one categorical factor. The main advantages of a CCD are its ability to efficiently fit a second-order polynomial model to capture nonlinear relationships and curvature, its flexibility in accommodating different numbers of factors, its efficiency in providing significant information on main effects, interactions, and quadratic terms with fewer runs than a full factorial design method. For the three numerical factors (extraction volumes, sample volume and pH) five levels (+1, −1, center point, +alpha and –alpha) were used, resulting in a complete design with 20 experimental points. This design includes 2^n ($2^3 = 8$) factor points, 2n ($2 \times 3 = 6$) axial points, 6 center points (six replicates) to optimize the values of these factors. The repetitions were done to minimize noise during actual experiments. The categorical factor (solvent type) had three levels (Methanol, Ethanol and ACN + Methanol). Incorporating the categorical factor into the optimization, multiplied the existing runs, leading to 60 runs. The selected parameter units and levels are shown in Table S2 all experiments were randomized. The experimental conditions and their outcomes are presented in Table S3. Analysis of variance (ANOVA) was performed on all the responses in the design to evaluate the statistical significance of the constructed models.

The results of the ANOVA for the developed models are presented in Tables S3-S6. Table S4, shows the ANOVA results for the proposed model for Imidacloprid (Rs1). The Model F-value of 623.45 indicates that the model is significant. In this case extraction volumes, sample volume, pH, type of solvent, and their interactions are significant model terms. Conversely, values greater than 0.050 indicate that the model terms are not significant. Additionally, the “Lack of Fit (LOF) *F*-value” of 2.1 shows that the LOF is not significant relative to the pure error.

For acetamiprid (Rs2), the variance analysis is shown in Table S5. Similar to imidacloprid (Rs1), the fitted model for acetamiprid (Rs2) is significance. The LOF *F*-value” of 1.38 indicates that the LOF is not significant. In this case, nearly all input variables have an influence on the acetamiprid response obtained by the regression model.

The variance analysis by ANOVA for carbendazim (Rs3) is shown in Table S6. The results showed that the proposed model is significant, and the LOF is not significant.

Table S7 presents the ANOVA results for the proposed model of thiacloprid (Rs4). The analysis reveals that the model is significant, and the LOF is not significant, suggesting a good fit to the data.

The most influential input variables in the regression model for thiacloprid response are extraction volume, sample volume, pH, and solvent type. This indicates that these variables significantly impact the thiacloprid response. Table S8 presents the statistical parameters obtained from ANOVA for the reduced models. In this case, both R^2 and adjusted R^2 values are greater than 0.99, indicating a very high level of model fit [35].

The adequate precision value measures the ‘signal (response) to noise (deviation) ratio’, with a ratio greater than 4 being desirable. In this study, the ratio ranged from 99.72 to 270.33, indicating strong signal and confirming that the model is significant for the extraction process.

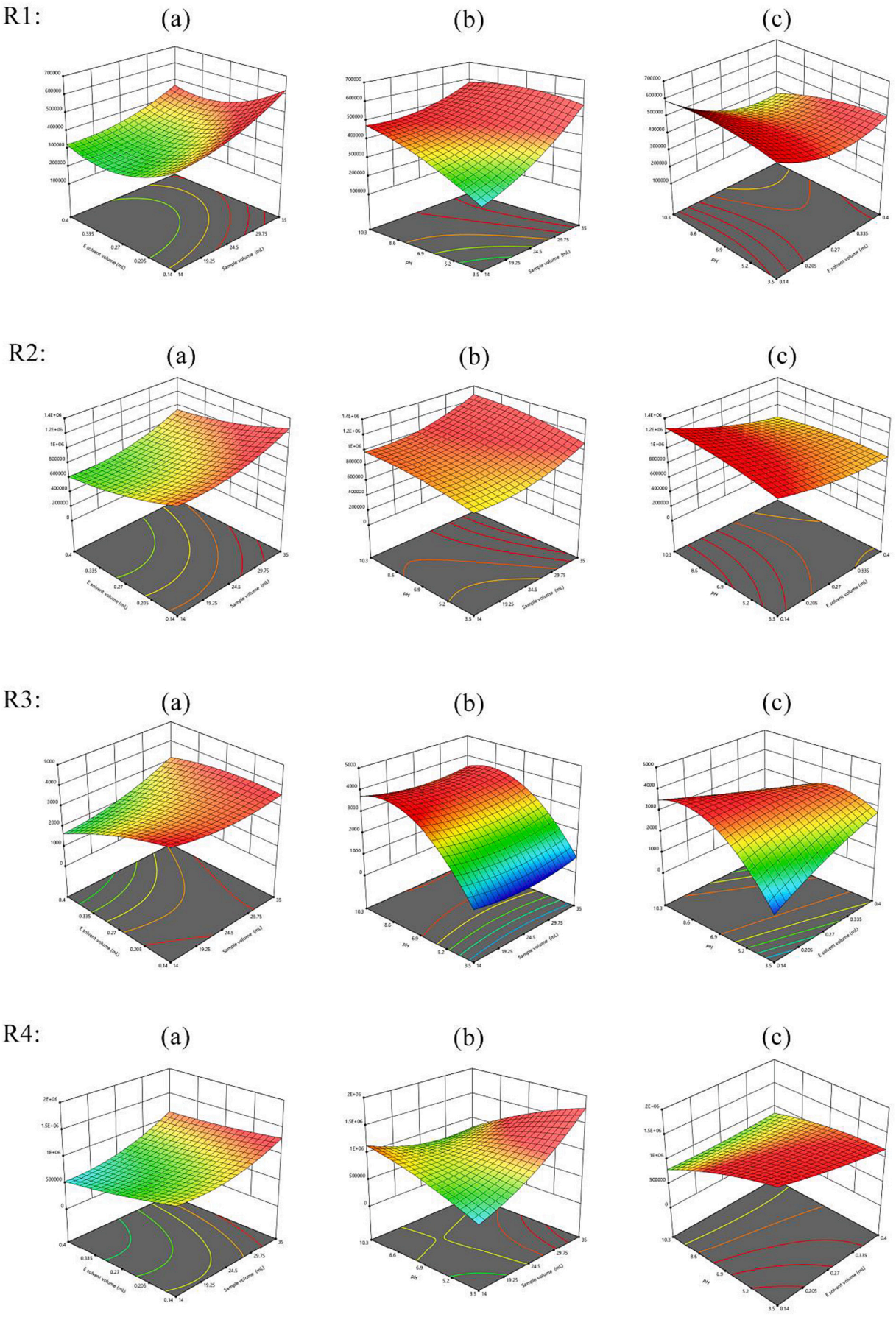

Fig. 2. Three-dimensional (3D) response surface for Imidacloprid (Rs1), Acetamiprid (Rs2), Carbendazim (Rs3) and Thiacloprid (Rs4).

Table 1.
The comparison of experimental and predictive of different objective functions under optimal conditions.

Optimum conditions	Sample Volume (mL)	Solvent Volume (mL)	pH	Solvent type	Rs_1	Rs_2	Rs_3	Rs_4
Desired value	34.7	0.22	7.25	ACN + Methanol				
Experimental					478,762	1,074,826	3598	1,194,083
Predictive					472,438	1,059,261	3595	1,210,063
% error					−1.3	−1.4	−0.08	1.3

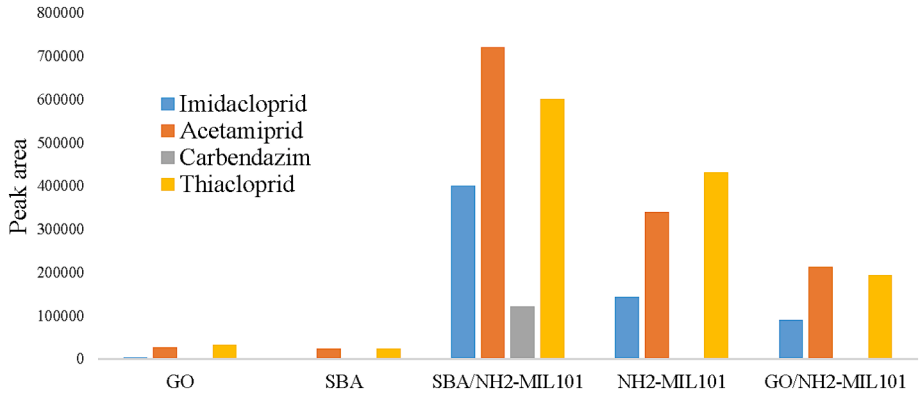

Fig. 3. Effects of adsorbent type on the extraction efficiencies of pesticides. Experimental condition: sample volume, 35.0 mL; flow rate of sample, 4.0 mL/min; desorption solvent, 0.22 mL ACN + methanol.

3.2.1. *Response surface methodology*

Design of experiment was employed to maximize the response for imidacloprid (Rs1), acetamiprid (Rs2), carbendazim (Rs3) and thiacloprid (Rs4). This approach helps to visualize the relationship between the responses and the experimental levels of each factor. The 3D response surface plots provide insights into the interaction between variables and their effect on the final model response. Fig. 2 displays the response surface plots as functions of two factors at a time, with all other factors held constant.

As shown in Fig. 2, the maximum extraction efficiency was achieved at a pH of around 7.5 for all the studied pesticides. To further investigate the effect of pH, the zeta potential of the synthesized adsorbents was measured at different pH values, and the results are presented in Fig. S5. As indicated, Cr-MOF and its nanocomposites exhibit a net positive charge at pH values below 7.5, a net negative charge above pH 8, and approximately zero net charge between 7.5 and 8. This behavior can be attributed to the formation of carboxylates under alkaline conditions and ammonium groups under acidic conditions in the linkers. Since the analytes are nonionic compounds, neutral pH values result in better extraction performance.

In addition, when the solvent volume was increased by 0.25 mL, a slight increase in the peak areas of the extracted pesticides was observed. However, further increases beyond 0.25 mL led to a decline in peak areas, which can be attributed to the limited adsorption capacity of the sorbent for each analyte. Consequently, additional solvent caused dilution of the analytes, resulting in smaller peaks. Therefore, 0.25 mL was selected as the optimal solvent volume for desorbing the target analytes from NH2-MIL-101(Cr)-SBA. As shown in Fig. 2, increasing the sample volume led to an increase in the peak areas of the extracted pesticides. This is expected, as a larger sample volume provides a higher amount of analyte available for adsorption or extraction.

The maximum responses were achieved with a sample volume of 34.7 mL, a solvent volume of 0.25 mL, a pH of 7.25 and a solvent mixture of acetonitrile and methanol. The individual response values corresponding to these optimized factors, for the four responses are presented in Table 1. The desirability obtained from the fitting is highly acceptable, given the simultaneous optimization of multiple responses. The suggested values were experimentally validated, and the agreement between experimental and predicted responses, including the percentage errors, is shown in Table 1. As can be seen, there is a good agreement between the experimental and predicted responses.

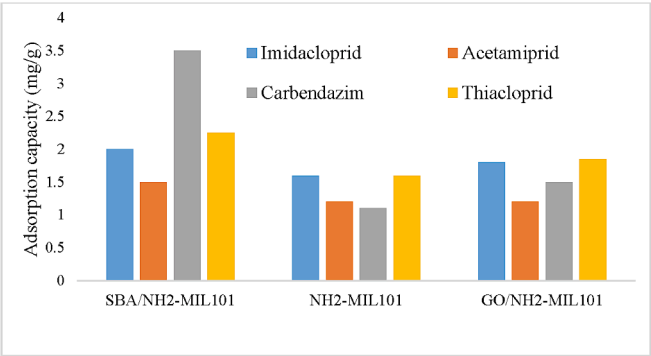

Fig. 4. Effect of adsorbent type on adsorbent capacity.

3.3. *Material selection*

Adsorption and desorption phenomena are two main practical factors that can impact the extraction efficiency of sorbent in SPE. The extraction efficiency of each of the synthesized composites and their components (GO, SBA, NH_2-MIL-101(Cr), NH_2-MIL-101(Cr)/GO and NH_2-MIL-101(Cr)/SBA) for the target pesticides was evaluated and the results are shown in Fig. 3. It was found that the extraction efficiency of NH_2-MIL101(Cr)-SBA was higher than that of NH_2-MIL-101(Cr) and the extraction efficiency of NH_2-MIL-101(Cr) was also higher than that of NH_2-MIL-101(Cr)/GO. NH_2-MIL-101(Cr) possesses valuable features such as a stable chemical structure, uniformly distributed pores with diameters greater than 4 nm, a remarkable surface area, and the presence of various functional groups, including carboxylate, phenyl, and amine moieties in its linker. These characteristics enhance the adsorption of organic analytes containing electronegative heteroatoms and aromatic rings. Therefore, when combined with other nanostructures

Table 2.
Method analytical performance of the target pesticides for river water.[c, d]

Sample	compounds	LOD (μg/L)	LOQ (μg/L)	LR (μg/L)	r^2	RSD%[a] intra-day	inter-day	ME%[b]	EF
River water	Imidacloprid	0.15	0.5	0.5–400.0	0.995	3.6	4.3	98	73
	Acetamiprid	0.07	0.25	0.25–300.0	0.995	2.8	3.7	100	129
	Carbendazim	0.6	2.0	2.0–800.0	0.995	3.9	5.0	97	84
	Thiacloprid	0.1	0.3	0.3–350.0	0.995	3.2	3.9	100	108

[c] RSDs, intra-day (n = 5) and inter-day within 3 days, 10.0 μg/L for water samples.
[d] matrix effect = 10.0 μg/L for water samples.

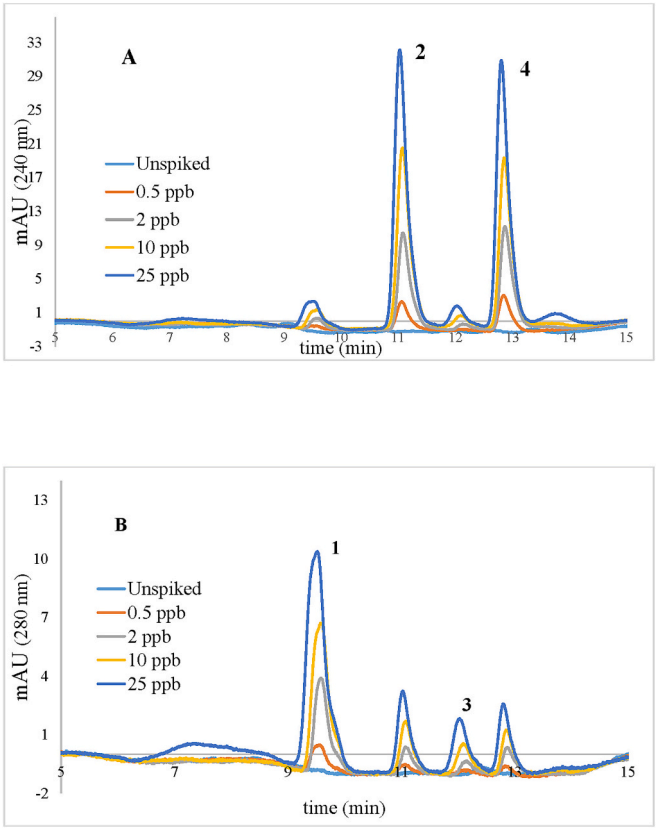

Fig. 5. HPLC-UV Chromatograms obtained in (A) river water (for detection wavelength 240 nm), (B) river water (for detection wavelength 280 nm); blank, 0.5, 2.0, 10.0 and 25.0 μg/L spiked concentration. 1. Imidacloprid; 2. Acetamiprid; 3. Carbendazim; 4. Thiacloprid.

such as SBA, NH_2-MIL-101(Cr) can provide improved adsorption performance for such analytes.

Hence, adsorption capacities of synthesized MOF and their nanocomposites were investigated, and the results are presented in Fig. 4. The obtained results demonstrated that SBA/MOF had a higher adsorption capacity than other adsorbents which was attributed to the synergistic effect of π-π interactions (between the benzene rings inside the pores of MOF and unsaturated bounds of pesticides), hydrogen bonding (between surface hydroxyls of SBA as HB donor and pesticides molecules as HB acceptor) and electrostatic attractions between nanocomposite and polar pesticides. The GO/MOF nanocomposite has a fewer surface hydroxyls groups than SBA/MOF sorbent and consequently has a lower adsorption capacity. But due to having flat benzene rings in the flexible structure of GO, it has a higher adsorption capacity than NH_2-MIL-101(Cr) MOF (Fig. 3). Additionally, due to having planar benzene rings in the flexible structure of GO and the formation of stronger π-π interactions, GO/MOF has a higher adsorption capacity than NH_2-MIL-101(Cr) MOF, but it has a lower desorption and consequently lowest amount of extraction (Fig. 4).

3.4. Method validation

The effectiveness of the syringe filter-SPE approach, employing the NH_2-MIL-101(Cr)/SBA composite as the adsorbent, was systematically assessed for the extraction of four pesticides: imidacloprid, acetamiprid, carbendazim, and thiacloprid. Key analytical parameters such as detection limits (LOD), quantification limits (LOQ), linear range, correlation coefficients (R^2), matrix effect percentages (ME%), enrichment factors (EFs), and precision expressed via relative standard deviations (RSDs) within and across days were thoroughly evaluated (see Table 2).

The procedure exhibited broad calibration ranges, spanning from 0.5 to 400 μg/L for imidacloprid, 0.25 to 300 μg/L for acetamiprid, 2 to 800 μg/L for carbendazim, and 0.3 to 350 μg/L for thiacloprid. All analytes showed excellent linearity with correlation coefficients nearing 0.995. Limits of detection, defined by a signal-to-noise ratio of 3, were 0.15 μg/L (imidacloprid), 0.07 μg/L (acetamiprid), 0.6 μg/L (carbendazim), and 0.1 μg/L (thiacloprid). Quantification thresholds, set at an S/N of 10, were determined as 0.5, 0.25, 2.0, and 0.3 μg/L, respectively. The method demonstrated robust repeatability, with intra-day RSDs ranging between 2.8 % and 3.9 % ($n = 5$) and inter-day RSDs falling between 3.7 % and 5.0 % ($n = 3$). Enrichment factors, reflecting the concentration amplification achieved by the sorbent relative to the original aqueous sample, were calculated to be 73 for imidacloprid, 129 for acetamiprid, 84 for carbendazim, and 108 for thiacloprid.

Table 3
Application of the nanocomposite as sorbent to determination of target pesticides in real samples.

	Imidacloprid				Acetamiprid				Carbendazim				Thiacloprid			
River water																
Added (μg/L)	0	2.0	6.0	40.0	0	2.0	6.0	40.0	0	2.0	6.0	40.0	0	2.0	6.0	40.0
Found (μg/L)	–	1.9	5.8	41.0	–	2.1	6.0	40.4	–	1.8	5.7	39.0	–	2.0	5.9	39.7
RR%	–	95.0	96.6	102.5	–	105.0	100.0	101.0	–	90.0	95.0	97.5	–	100.0	98.3	99.2
Well water																
Added(μg/L)	0	2.0	6.0	40.0	0	2.0	6.0	40.0	0	2.0	6.0	40.0	0	2.0	6.0	40.0
Found (μg/L)	–	1.9	5.9	40.6	–	2.1	6.1	39.5	–	1.8	5.8	39.7	–	1.9	6.0	40.0
RR%	–	95.0	98.3	101.5	–	105.0	101.6	98.7	–	90.0	96.6	99.2	–	95.0	100.0	100.0

Table 4
Comparison of the current method with other reported techniques for pesticides analysis.

Method	Adsorbent	Analyte	sample	LOD µg/L	R% %	LR µg/L	RSD %	Solvent (mL)	Ref
SPE-HPLC-DAD	(MIL-53(Al) @cellulose paper	(Neonicotinoids) thiamethoxam, clothianidin, imidacloprid, acetamiprid, and thiacloprid	environmental water	1.0–1.6	81–114	3–500	3.6–5.6	Acetonitrile (1 mL)	[8]
MSPE/(HPLC-MS/MS)	MOF-199/Fe3O4	(Neonicotinoids) dinotefuran, thiamethoxam, clothianidin, acetamiprid, nitenpyram, imidacloprid and thiacloprid	Environmental water	0.3–1.5	88.0 to 107.0	2–800	1.5 to 11.6	Acetone	[35]
DSPE/(HPLC-MS	MOF- UIO-66	(Neonicotinoids) thiamethoxam, clothianidin, acetamiprid, imidacloprid and thiacloprid	Environmental water	0.02–0.4	73.7–119.0,	10–500	2.4 and 17.1	Acetone	[36]
SPE-HPLC-DAD	(ZIF-8) MOF with AuNPs	(Neonicotinoids) thiamethoxam, clothianidin, acetamiprid, imidacloprid and thiacloprid	River water and agave syrup	0.019 to 0.041	80 and 110	1–5000	<10	MeOH:H2O (60:40, v:v)	[37]
(UA-MSPE)-HPLC-DAD	MIL-101 (Cr)-NH2 (MGO/MIL)	(Neonicotinoids) Acetamiprid and Imidacloprid	Fruit and water sample	0.022–0.019	82.13 to 102.27	0.064–3500	3.93–8.50	ethylamine/ethanol	[38]
MSPE-HPLC-UV	(MOPC–ZSM-5) sorbent	(Neonicotinoids) (acetamiprid, imidacloprid, thiacloprid and thiamethoxam	water and peanut milk samples	0.1–2.0	96.74–112.4	0.5–1000	5.2–7.4	acetonitrile	[39]
SPE/HPLC-PDA	NH2-MIL101 (Cr)-SBA-15"	(Neonicotinoids) acetamiprid, Imidacloprid, carbendazim and thiacloprid	River water	0.07–0.15	90–105	0.25–800	2.8–5.0	methanol: ACN (20:80) 0.22	This study

3.5. Selectivity and matrix effect

The selectivity of the proposed method was examined by evaluating possible interference from substances likely to be present with the target pesticides, following FDA validation guidelines [29]. As depicted in Fig. 5, analysis of pesticide-free river water revealed no significant peaks that could interfere, confirming excellent selectivity and clear chromatographic separation of the pesticides (Fig. 3B). In addition, the impact of sample matrix on the analytical signal, known as the matrix effect (ME%), was investigated by comparing measurements from samples before and after spiking with analytes. The matrix effect was calculated using the formula below [27]:

$$ME\% = \frac{A_S - A_n}{A_w} \times 100.$$

where As, An, and Aw correspond to the peak area of the analyte in the spiked, non-spiked samples, and spiked ultra-pure water, respectively. As shown in Table 2, the proposed method does not experience significant matrix effects when analyzing the studied pesticides in real samples.

3.6. Real sample analysis

The proposed method was applied to analyze four pesticides in two different water samples, river water and well water, to evaluate its effectiveness for real-world applications. The results are summarized in Table 3. The real samples were spiked with target pesticides at concentration levels ranging from 1.0 to 40.0 µg/L and HPLC-PDA analysis was conducted to examine the method accuracy. The recoveries, which ranged from 95 % to 105 % confirms the method's reliability for pesticide detection in water samples (Table 2). The HPLC-PDA chromatograms obtained are displayed in Fig. 5.

4. Comparison study

Table 4 provides a comparative overview of the newly developed syringe filter-SPE against various existing SPE techniques for extracting and analyzing neonicotinoid insecticides. The new approach demonstrated lower relative standard deviations (RSDs) than most other methods, indicating enhanced precision. Additionally, its limits of detection (LODs) were comparable with or better than those reported by alternative procedures. These results suggest that the NH2-MIL101(Cr)-SBA-15 sorbent-based syringe filter-SPE is a reliable, accurate, and reproducible technique suitable for concentrating and measuring neonicotinoid insecticides across different sample matrices.

5. Conclusion

This study presents the development and application of a novel nanocomposite, SBA/NH_2-MIL-101(Cr), as a high-performance metal-organic framework for the selective extraction and quantification of four pesticides from environmental water samples using a syringe filter-based solid-phase extraction (SPE) approach. The NH_2-MIL-101(Cr) component exhibited excellent affinity for the target pesticides and operated efficiently in the SPE setup without causing back pressure. Incorporating SBA into the composite significantly enhanced its adsorption capacity. Integrating the composite into a syringe filter device enabled rapid extractions and markedly lowered the limits of quantification (LOQs), offering practical advantages for processing larger sample volumes. The method demonstrated strong reproducibility and achieved low detection thresholds for all four analytes. Furthermore, the use of SBA/NH_2-MIL-101(Cr) minimized solvent consumption while improving the extraction efficiency, especially for more hydrophobic pesticides. However, one of the disadvantages that can be mentioned in this work is that the volume of desorbtion solvent cannot be reduced below the optimum volume (220 µL) due to the high volume and surface of the commercially syringe filters. Whereas, if smaller filters are made, both solvent and adsorbent consumption can be reduced and the enrichment factor can be increased. This work suggests that the proposed technique holds significant promise for future trace-level analysis of a broader range of pesticides and organic contaminants in complex environmental matrices.

CRediT authorship contribution statement

Soleyman Moinfar: Writing – original draft, Supervision, Resources, Project administration, Investigation, Funding acquisition, Data curation, Conceptualization. **Ali Khodayari:** Writing – original draft, Visualization, Validation, Investigation, Data curation, Conceptualization. **Aveen Mustafa Mohammed:** Writing – original draft, Methodology. **Eslam Pourbasheer:** Writing – original draft, Software, Formal analysis. **Ali Aghaei:** Writing – review & editing, Investigation.

Declaration of competing interest

The authors declare that they have no known competing financial interests or personal relationships that could have appeared to influence the work reported in this paper.

Acknowledgments

The authors gratefully acknowledge the financial support of the University of Zakho, Iraq.

Appendix A. Supplementary data

Supplementary data to this article can be found online at https://doi.org/10.1016/j.microc.2025.115322.

Data availability

No data was used for the research described in the article.

References

[1] W. Li, T. Jinyu, W. Zhonggang, Micro−/mesoporous fluorescent polymers and devices for visual pesticide detection with portability, high sensitivity, and ultrafast response, ACS Appl. Mater. Interfaces 14 (2022) 5815–5824, https://doi.org/10.1021/acsami.1c21658.

[2] O. Ozalp, G.Z. Pinar, S. Mustafa, MIL-101 (Cr) metal–organic frameworks based on deep eutectic solvent (ChCl: urea) for solid phase extraction of imidacloprid in tea infusions and water samples, J. Mol. Liq. 378 (2023) 121589, https://doi.org/10.1016/j.molliq.2023.121589.

[3] B. Yang, W. Ma, S. Wang, L. Shi, X. Li, Z. Ma, Q. Zhang, H. Li, Determination of eight neonicotinoid insecticides in Chinese cabbage using a modified QuEChERS method combined with ultra-performance liquid chromatography-tandem mass spectrometry, Food Chem. 387 (2022) 132935, https://doi.org/10.1016/j.foodchem.2022.132935.

[4] M.L. Hladik, A.R. Main, D. Goulson, Environmental risks and challenges associated with neonicotinoid insecticides, Environ. Sci. Technol. 52 (2018) 3329–3335, https://doi.org/10.1021/acs.est.7b06388.

[5] P. Yin, Y. Dong, X. Zhou, Q. Wang, S. Li, C. Wang, L. Hao, Z. Wang, Q. Wu, Synthesis of phosphate-functionalized magnetic porous organic polymer: a sorbent for sensitive determination of neonicotinoid insecticides in water and lemon juice, J. Chromatogr. A 1705 (2023) 464221, https://doi.org/10.1016/j.chroma.2023.464221.

[6] A. Lentola, C. Giorio, S. Bogialli, M. Roverso, M. Marzaro, V. Girolami, A. Tapparo, Methiocarb metabolites are systemically distributed throughout corn plants grown from coated seeds, Environ. Chem. Lett. 19 (2021) 1887–1892, https://doi.org/10.1007/s10311-020-01098-3.

[7] J. Lämsä, E. Kuusela, J. Tuomi, S. Juntunen, P.C. Watts, Low dose of neonicotinoid insecticide reduces foraging motivation of bumblebees, Proc. R. Soc. B Biol. Sci. 285 (2018) 0506, https://doi.org/10.1098/rspb.2018.0506.

[8] S. Singh, N. Singh, V. Kumar, S. Datta, A.B. Wani, D. Singh, K. Singh, J. Singh, Toxicity, monitoring and biodegradation of the fungicide carbendazim, Environ. Chem. Lett. 14 (2016) 317–329, https://doi.org/10.1007/s10311- 016-0566-2.

[9] E.M. Rama, S. Bortolan, M.L. Vieira, D.C.C. Gerardin, E.G. Moreira, Reproductive and possible hormonal effects of carbendazim, Regul. Toxicol. Pharmacol. 69 (2014) 476–486, https://doi.org/10.1016/j.yrtph.2014.05.016.

[10] M.Romagnoli, A. Scarparo, M. Catani, B. Giannì, L. Pasti, A. Cavazzini, and F.A. Franchina, Development and validation of a GC× GC-ToFMS method for the quantification of pesticides in environmental waters, Anal. Bioanal. Chem., 415 (2023) 4545–4555. https:// https://doi.org/10.1007/s00216-023-04686-8.

[11] Directive (EU) 2020/2184 of the European Parliament and of the Council of 16 December 2020 on the quality of water intended for human consumption, Official Journal of the European Union. L 435 (23 December 2020) 1–62. https://eur-lex.europa.eu/eli/dir/2020/2184/oj.

[12] European Parliament and Council, Directive 2006/118/EC of 12 December 2006 on the protection of groundwater against pollution and deterioration, Off. J. Eur. Union L 372/19 (2006). Accessed April 22, 2025, https://eur-lex.europa.eu/legal-content/EN/TXT/?uri=celex%3A32006L0118.

[13] A.R. Bagheri, A. Shokrollahi, Chitosan composited covalent organic framework nanoparticles for the dispersive micro-solid-phase extraction of chlorpyrifos pesticide from environmental water samples prior to spectrophotometric determination, Microchem. J. 211 (2025) 113153, https://doi.org/10.1016/j.microc.2025.113153.

[14] Z.L. Li, X.R. Qi, Y.H. Xu, J.Q. Zhao, G.F. Zuo, M.M. Wang, Highly efficient and convenient QuEChERS using ZIF-67 derived magnetic nanoporous carbon for determination of carbamate pesticides in various vegetable and fruit samples, Food Chem. 472 (2025) 142904, https://doi.org/10.1016/j.foodchem.2025.142904.

[15] A.T. Cardoso, F.M. Lanças, Graphene oxide functionalized with hydrophilic ionic liquid as stir bar coating: Sorptive extraction of selected triazines in grape juice samples, Anal. Chim. Acta 343 (2025) 343691, https://doi.org/10.1016/j.aca.2025.343691.

[16] A. Ghiasi, A. Malekpour, S. Mahpishanian, Metal-organic framework MIL101 (Cr)-NH2 functionalized magnetic graphene oxide for ultrasonic-assisted magnetic solid phase extraction of neonicotinoid insecticides from fruit and water samples, Talanta 217 (2020) 121120, https://doi.org/10.1016/j.talanta.2020.121120.

[17] H. Mahmoudi-Moghaddam, H.A. Javar, Z. Garkani-Nejad, Fabrication of platinum-doped NiCo2O4 nanograss modified electrode for determination of carbendazim, Food Chem. 383 (2022) 132398, https://doi.org/10.1016/j.foodchem.2022.132398.

[18] Y. Yang, Y. Guo, X. Jia, Q. Zhang, J. Mao, Y. Feng, D. Yin, W. Zhao, Y. Zhang, G. Ouyang, W. Zhang, An ultrastable 2D covalent organic framework coating for headspace solid-phase microextraction of organochlorine pesticides in environmental water, J. Hazard. Mater. 452 (2023) 131228, https://doi.org/10.1016/j.jhazmat.2023.131228.

[19] H. Huang, N. Li, Y. Chen, X. Shentu, X. Yu, Z. Ye, Synthesis of multiwalled carbon nanotubes/metal-organic framework composite for the determination of neonicotinoid pesticides in medicine and food homology products, Food Chem. 434 (2024) 137354, https://doi.org/10.1016/j.foodchem.2023.137354.

[20] S. Moinfar, A. Khodayari, S.S. Abdulrahman, A. Aghaei, S. Sohrabnezhad, L. A. Jamil, Development of a SPE/GC–MS method for the determination of organophosphorus pesticides in food samples using syringe filters packed by GNP/MIL-101 (Cr) nanocomposite, Food Chem. 371 (2022) 130997, https://doi.org/10.1016/j.foodchem.2021.130997.

[21] S. Moinfar, A. Khodayari, H.Z. Sami, M.K. Ali, N.N. Abdi, Investigation of five metal–organic frameworks as sorbents in the syringe filter-SPE method for determination of metronidazole and cephalexin in water samples, New J. Chem. 46 (2022) 10308–10316, https://doi.org/10.1039/D2NJ00907B.

[22] S. Huang, G. Chen, N. Ye, X. Kou, F. Zhu, J. Shen, G. Ouyang, Solid-phase microextraction: An appealing alternative for the determination of endogenous substances-a review, Anal. Chim. Acta 1077 (2019) 67–86, https://doi.org/10.1016/j.aca.2019.05.054.

[23] A. Modrow, D. Zargarani, R. Herges, N. Stock, Introducing a photo-switchable azo-functionality inside Cr-MIL-101-NH 2 by covalent post-synthetic modification, Dalton Trans. 41 (2012) 8690–8696, https://doi.org/10.1039/C2DT30672G.

[24] X.L. Wang, H.L. Fan, Z. Tian, E.Y. He, Y. Li, J. Shangguan, Adsorptive removal of sulfur compounds using IRMOF-3 at ambient temperature, Appl. Surf. Sci. 289 (2014) 107–113, https://doi.org/10.1016/j.apsusc.2013.10.115.

[25] N. Tian, Q.M. Jia, H.Y. Su, Y.F. Zhi, A.H. Ma, J. Wu, S.Y. Shan, The synthesis of mesostructured NH 2-MIL-101 (Cr) and kinetic and thermodynamic study in tetracycline aqueous solutions, J. Porous. Mater. 23 (2016) 1269–1278, https://doi.org/10.1007/s10934-016-0186-z.

[26] T. Wang, P. Zhao, N. Lu, H. Chen, C. Zhang, H. Xiaohong, Acile fabrication of Fe3O4/MIL-101 (Cr) for effective removal of acid red 1 and orange G from aqueous solution, Chem. Eng. J. 295 (2016) 403–413, https://doi.org/10.1016/j.cej.2016.03.016.

[27] Y. Jafari-Tarzanagh, D. Seifzadeh, A. Khodayari, R. Samadianfard, Active corrosion protection of AA2024 aluminum alloy by sol-gel coating containing inhibitor-loaded mesoporous SBA-15, Prog. Org. Coat. 173 (2022) 107166, https://doi.org/10.1016/j.porgcoat.2022.107166.

[28] U. Kanta, V. Thongpool, W. Sangkhun, N. Wongyao, J. Wootthikanokkhan, Preparations, characterizations, and a comparative study on photovoltaic performance of two different types of graphene/TiO2 nanocomposites photoelectrodes, J. Nanomater. 2017 (2017) 2758294, https://doi.org/10.1155/2017/2758294.

[29] S Moinfar, A Khodayari, HZ Sami, MK Ali, and N.N. Abdi, Investigation of five metal–organic frameworks as sorbents in the syringe filter-SPE method for determination of metronidazole and cephalexin in water samples, New J. Chem., 46 (2022) 10308–10316. doi:https://doi.org/10.1039/D2NJ00907B.

[30] S. Wang, B. Ye, C. An, J. Wang, Q. Li, H. Guo, J. Zhang, Exploring the coordination effect of GO@ MOF-5 as catalyst on thermal decomposition of ammonium perchlorate, Nanoscale Res. Lett. 14 (2019) 345, https://doi.org/10.1186/s11671-019-3163-z.

[31] Y. Luan, Y. Qi, H. Gao, R.S. Andriamitantsoa, N. Zheng, G. Wang, A general post-synthetic modification approach of amino-tagged metal–organic frameworks to access efficient catalysts for the Knoevenagel condensation reaction, J Mater Chem A 3 (2015) 17320–17331, https://doi.org/10.1039/C5TA00816F.

[32] A. Kumar, A.M. Sadanandhan, S.L Jain, Retracted article: silver doped reduced graphene oxide as a promising plasmonic photocatalyst for oxidative coupling of benzylamines under visible light irradiation, New J. Chem., 43 (2019) 9116–9122. doi:https://doi.org/10.1039/C9NJ00852G.

[33] X. Luo, T. Shen, L. Ding, W. Zhong, J. Luo, Sh. Luo, Novel thymine-functionalized MIL-101 prepared by post-synthesis and enhanced removal of Hg2+ from water,

J. Hazard. Mater. 306 (2016) 313–322, https://doi.org/10.1016/j.jhazmat.2015.12.034.
[34] S. Wang, L. Bromberg, H. Schreuder-Gibson, T.A. Hatton, Organophophorous ester degradation by chromium (III) terephthalate metal–organic framework (MIL-101) chelated to N, N-dimethylaminopyridine and related aminopyridines, ACS Appl. Mater. Interfaces 5 (2013) 1269–1278, https://doi.org/10.1021/am302359b.
[35] X. Cao, G. Liu, Y. She, Z. Jiang, F. Jin, M. Jin, P. Du, F. Zhao, Y. Zhang, J. Wang, Preparation of magnetic metal organic framework composites for the extraction of neonicotinoid insecticides from environmental water samples, RSC Adv. 6 (2016) 113144–113151, https://doi.org/10.1039/C6RA23759B.
[36] X Cao, Z Jiang, S Wang, S Hong, H Li, C Zhang, Y. Shao, Y. She, F. Jin, M. Jin, J. Wang, Metal-organic framework UiO-66 for rapid dispersive solid phase extraction of neonicotinoid insecticides in water samples, J. Chromatogr. B, 1077 (2018) 92–97. doi:https://doi.org/10.1016/j.jchromb.2017.11.034.
[37] H. Martínez-Pérez-Cejuela, K. Pravcová, L. Česlová, E.F. Simó-Alfonso, J. M. Herrero-Martínez, Zeolitic imidazolate framework-8 decorated with gold nanoparticles for solid-phase extraction of neonicotinoids in agricultural samples, Microchim. Acta 188 (2021) 197, https://doi.org/10.1007/s00604-021-04872-4.
[38] M. Catalá-Icardo, C. Gómez-Benito, H. Martínez-Pérez-Cejuela, E.F. Simó-Alfonso, J.M. Herrero-Martínez, Green synthesis of MIL53 (Al)-modified paper-based analytical device for efficient extraction of neonicotinoid insecticides from environmental water samples, Anal. Chim. Acta 1316 (2024) 342841, https://doi.org/10.1016/j.aca.2024.342841.
[39] L. Liu, Y. Hao, X. Zhou, C. Wang, Q. Wu, Z. Wang, Magnetic porous carbon based solid-phase extraction coupled with high performance liquid chromatography for the determination of neonicotinoid insecticides in environmental water and peanut milk samples, Anal. Methods 7 (2015) 2762–2769, https://doi.org/10.1039/C4AY02990A.